Proceedings of ASME Turbo Expo 2014: Turbine Technical Conference and Exposition
GT2014
June 16 – 20, 2014, Düsseldorf, Germany

GT2014-27123

DRAFT

A SOOT CHEMISTRY MODEL THAT CAPTURES FUEL EFFECTS

Karthik V. Puduppakkam
Reaction Design
San Diego, California, USA

Abhijit U. Modak
Reaction Design
San Diego, California, USA

Chitralkumar V. Naik
Reaction Design
San Diego, California, USA

Ellen Meeks
Reaction Design
San Diego, California, USA

ABSTRACT

A detailed chemistry model is necessary to simulate the effects of variations in fuel composition on soot emissions. In this work, we have developed a detailed chemistry model for the soot formation and oxidation chemistry, with a focus on the surface kinetics of the soot-particle. Through collaboration with the University of Southern California (USC), the model has been compared to a unique set of soot particle-size data measured in flames for several single-component fuels. Fuel components used in the experiments represent the chemical classes found in jet, gasoline, and diesel fuels, including *n*-heptane (representative of *n*-alkanes) and toluene (aromatic). Measurements were taken in burner-stabilized stagnation-flame (BSSF) experiments, which can be simulated well using the 1-dimensional BSSF flame model in CHEMKIN-PRO. Soot volume fraction and particle size distributions are modeled using the sectional method option for Particle Tracking, within CHEMKIN-PRO software. The well-characterized flow of the BSSF experiments allows the modeling to focus on the kinetics. Validated detailed reaction mechanisms for fuel combustion and PAH production, combined with the new soot surface-kinetics mechanism, were used in the simulations. Simulation results were compared to measurements for both particle size distributions and total soot volume fraction. Observed effects of fuel, temperature, pressure, equivalence ratio and residence time on the soot size distribution shape and soot quantity were reproduced by the model.

The chemistry in the soot surface model includes particle nucleation, growth through the HACA (hydrogen-abstraction/carbon-addition) and PAH-condensation (polycyclic aromatic hydrocarbons) pathways, as well as soot-oxidation pathways. In addition to soot chemistry, the physics of particle coagulation and aggregation were included in the model. The results demonstrate the ability of well-validated chemistry to predict both dramatic and subtle effects related to soot mass and soot particle size.

INTRODUCTION

With stricter emissions standards and increased fuel composition variability, reducing soot emissions from jet or stationary gas-turbine engines remains a challenge. Soot formation and destruction is a complex phenomenon, which is driven by chemistry in the gas-phase and soot particle surface, and by the physics of flow in the combustor. In advanced gas turbine designs such as the Rich-Burn/Quick-Mix/Lean-Burn (RQL) combustion approach [1], significant amounts of soot can still potentially be formed in the fuel-rich sections due to poor fuel-air mixing.

The goal of this work has been to improve on the recent advances in the field to better simulate soot evolution in combustors. In particular, we wanted to accurately capture fuel effects and the effects on soot evolution of a wide range of operating conditions that changed temperature, equivalence ratio, pressure and residence time. Factors that have significant impact on the accuracy of soot predictions include the surrogate-fuel blend and the chemistry occurring in the gas-phase and on the surface of soot particles.

Fuel surrogate

A surrogate fuel, as the name implies, is a model fuel that emulates the necessary characteristics of the real fuel.

Consequently, the surrogate fuel must represent various chemical classes ranging from *n*-alkanes to aromatics in order to correctly capture the chemical effects. Since each individual component has a different sooting propensity [2], the components selection directly impacts soot-related predictions. Recommendations have been published for assembling multi-component surrogates for jet fuels [3], gasoline [4] and diesel [5]. As a part of work supported by the Model Fuels Consortium [6-11], we have developed a palette of 57 surrogate fuel components relevant to natural gas, syngas, gasoline, diesel, jet fuels, and biofuels. From this palette of surrogate components, we have developed a methodology and software for assembling surrogate fuels such that they match real-fuel properties [9, 12]. Targeted real-fuel properties include sooting tendency (as represented by H/C ratio of fuel and/or threshold sooting index), cumulative heat release (lower heating value), distillation curve, combustion dynamics (octane or cetane number), and structural information (content of aromatics, etc.).

As a first step towards predictive capability for surrogate-fuel combustion, it is essential to verify predictions for pure components from different chemical classes. In this work, the sooting behavior has been tested for the combustion of surrogate components that represent the major chemical classes.

Gas-phase mechanism

After assembling an accurate multi-component surrogate for a targeted fuel, the next challenge is constructing the corresponding reaction mechanism. We have developed and validated a detailed reaction mechanism as part of work supported by the Model Fuels Consortium [6-11]. This mechanism includes the reaction pathways for all 57 surrogate components; employing self-consistent and rules-based reaction rates. The reaction mechanism has 8460 species and 34027 reactions.

For predicting the soot precursors, it is important to accurately represent small hydrocarbons, such as acetylene, in the gas-phase mechanism. Towards this end, the core chemistry of our mechanism was recently updated and validated over a wide range of conditions [10, 11]. In addition to the core chemistry, it is well documented in the literature that polycyclic aromatic hydrocarbon (PAH) species are important soot precursors [13-16]. The gas-phase mechanism includes PAH species up to the 4-ring molecule pyrene.

Soot surface mechanism

From the gas-phase soot precursors, soot particles can nucleate, grow, and oxidize through multiple parallel pathways. Table 1 lists all the reaction pathways in our soot surface mechanism. The mechanism considers soot nucleation from pyrene, acenaphthalene, naphthalene, benzene and acetylene. Soot growth can occur through the HACA (hydrogen-abstraction/carbon-addition) and PAH-condensation (polycyclic aromatic hydrocarbons) routes. This involves the precursor species acetylene, propargyl radical, benzene, toluene, acenaphthalene and pyrene. Soot oxidation can occur through reactions with molecular oxygen and hydroxyl radical. Based on some recent experimental data from USC, nascent soot was found to be oxidized by molecular oxygen at a rate substantially larger than that described by the classical Nagle-Strickland Constable (NSC) empirical equation [17]. Additionally, the mechanism also considers active and inactive sites on the soot surface; open(s) in Table 1 is an inactive surface site, while open(se) and h(se) are active sites. In Table 1, soot is represented as C_B. The total number of sites from nucleation reactions is based on the surface site density used of 3.3×10^{-9} moles/cm^2.

Table 1: List of soot surface reactions

Type	Reaction
Nucleation	pyrene + pyrene $\rightarrow$ $32C_B$ + 28.72open(se) + 20H(se)
Nucleation	pyrene + acenaphthalene $\rightarrow$ $28C_B$ + 26.57open(se) + 18H(se)
Nucleation	pyrene + naphthalene $\rightarrow$ $26C_B$ + 24.4open(se)+ 18H(se)
Nucleation	pyrene + benzene $\rightarrow$ $22C_B$ + 21.9open(se) + 16H(se)
Nucleation	pyrene + acetylene $\rightarrow$ $18C_B$ + 21.2open(se) + 12H(se)
Site conversion	open (se) $\leftrightarrow$ open(s)
Site conversion	H(se) $\rightarrow$ $0.5H_2$ + open(se)
Soot growth	open(se) + acetylene $\rightarrow$ $2C_B$ + H_2 + open(s)
Soot growth	open(se) + propargyl $\rightarrow$ $3C_B$ + $1.5H_2$ + open(s)
Soot growth	open(se) + pyrene $\rightarrow$ $16C_B$ + $5H_2$ +open(s)
Soot growth	open(se) + acenaphthalene $\rightarrow$ $12C_B$ + $4H_2$ + open(s)
Soot growth	open(se) + toluene $\rightarrow$ $7C_B$ + 4 hydrogen+ open(s)
Soot growth	open(se) + benzene $\rightarrow$ $6C_B$ + 3 hydrogen + open(s)
Soot oxidation	open(se) + hydroxyl + C_B $\rightarrow$ CO + 0.5 hydrogen + open(se)
Soot oxidation	open(se) + oxygen + C_B $\rightarrow$ CO + 0.5 oxygen + open(se)

This accurate soot chemistry model can be used directly in CFD with a particle-tracking method [18], or as part of the Equivalent reactor network approach [19, 20].

MODELING AND VALIDATION

In this section, simulation results are compared to experimental data; first for nucleation and growth regimes, and then for soot oxidation. The growth-related data come from

burner-stabilized stagnation-flames (BSSF) experiments, flow reactors, and shock-tube reactors.

Mechanism Reduction

It is computationally expensive to use the full (8460 species) mechanism mentioned above in flame simulations. For the work reported here, a targeted mechanism reduction was performed using the Reaction Workbench software [12]. During the mechanism reduction, it was prescribed that the discrepancy between predictions using the master and reduced mechanisms for the soot-precursor species acetylene, propargyl radical, benzene, toluene, naphthalene, acenaphthalene and pyrene, be within an absolute tolerance of 1 ppm, and a relative tolerance of 10% for all of the targeted conditions. Therefore, the reduced mechanism performed accurately relative to the master mechanism for the soot precursors over the conditions of interest. Figure 1 shows an example comparison for a toluene BSSF flame, where the predictions with the reduced mechanism are in a very good agreement with those obtained with the master mechanism. Separate reduced mechanisms were generated for ethylene, *n*-heptane, and toluene.

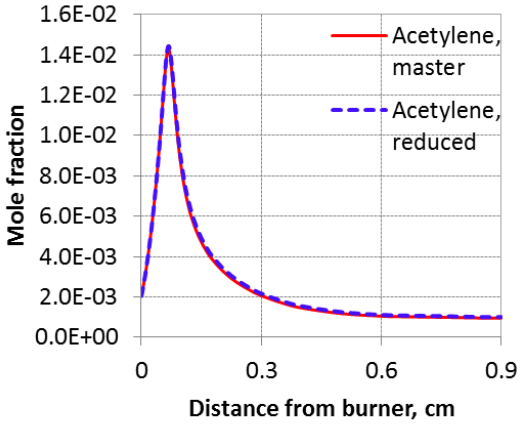

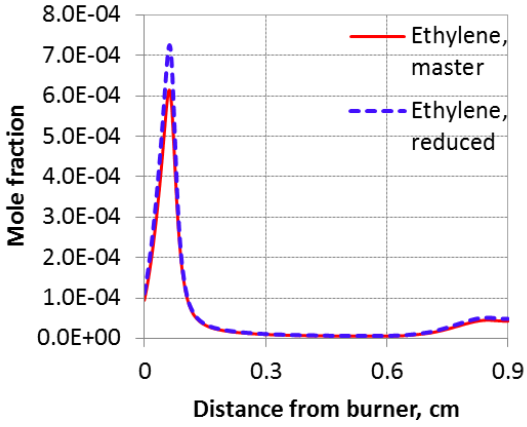

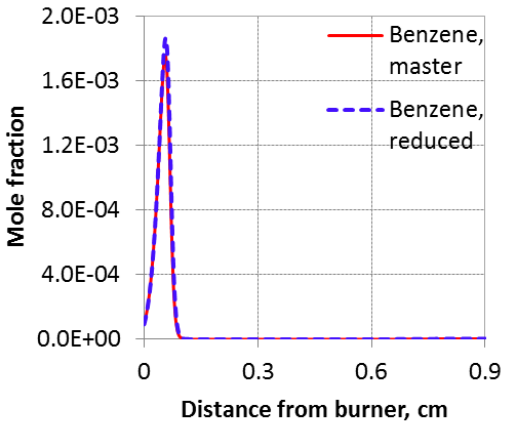

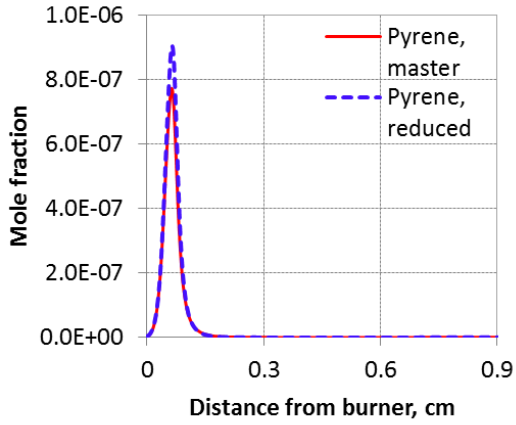

Figure 1: An example showing the accuracy of the reduced gas-phase mechanism, in comparison with the master mechanism, for a toluene BSSF flame.

Soot nucleation and growth

Validation using burner-stabilized stagnation-flame (BSSF) data

Soot measurements in burner-stabilized flame experiments typically involve some inaccuracies due to the use of invasive soot probes. The burner-stabilized stagnation-flame (BSSF) experimental setup developed at the University of Southern California addresses this issue [21, 22]. Figure 2 shows a schematic of the BSSF experiment. In this setup, the soot probe is embedded in a stagnation plane which eliminates the probe perturbations of the flame itself. In addition, from a modeling perspective the boundary conditions of this stagnation plane are well-defined and hence this setup can be simulated with high fidelity with respect to the fluid dynamics. More details regarding the experimental setup can be found in references [21, 22]. The model treats the stagnation plane as a wall boundary, assuming no-slip convective velocity condition, and also assuming that the species convective and diffusive fluxes balance. The experimentally measured burner inlet temperature and the stagnation plane temperature are used in the simulations as boundary conditions.

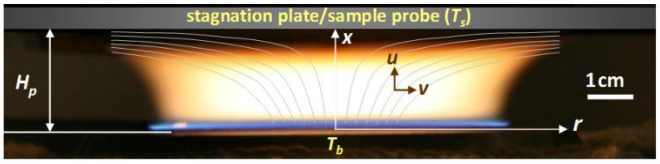

Figure 2: Schematic of the BSSF experiment

The 1-dimensional CHEMKIN-PRO BSSF model [23] was developed to simulate such experiments. Through collaboration with the University of Southern California, the soot model has been compared to a unique set of soot data measured in flames for several single-component fuels. Fuel components used in the experiments represent the chemical classes found in jet, gasoline, and diesel fuels. This section discusses a few sets of these data, as listed in Table 2. The sectional model option was used for the particle tracking, with diameters ranging up to 24 μm and a section spacing factor of 2. Gas-phase radiation effects have been considered using the optically-thin model in the BSSF simulations, along with soot particle radiation.

Soot particle aggregation has also been modeled. The essential properties of an aggregate can be obtained from two parameters: the number of primary particles and the fractal dimension. In general, the particle material's sintering data is required in order to capture the evolution of particle aggregates. The complete aggregation model from CHEMKIN-PRO uses such sintering data and can model the details of aggregate dynamics. However, such data is not readily available for soot particles. Consequently, in the results reported here, the simple aggregation model from CHEMKIN-PRO is used. In contrast to the complete aggregation model, the simple model uses user-specified primary particle diameter and fractal dimension as input. The formulation of the simple model is motivated by the fact that the characteristic sintering time has a power law dependence of order 4 on primary particle diameter. This indicates that aggregates with small primary particles coalesce quickly whereas those with larger particles will take a long time thus resulting in a limiting primary particle size. In other words, the system of particles will consist of completely coalesced spheres below a limiting size and pure aggregates that contain primary particles of the liming size. With pre-specified primary particle diameter and fractal dimension, the simple model can hence calculate a better estimate of the collision diameter and hence allow incorporation of aggregation dynamics. It should be noted that with the simple model one still solves for particle nucleation, collision, and growth. When the volume averaged diameter is less than the specified primary particle diameter it is assumed that the aggregate is completely coalesced otherwise it is assumed to be a pure aggregate. In the simulation results reported, the primary particle diameter of 20 nm is used along with a fractal dimension of 1.8. The former choice is influenced by experimental results whereas the latter value is typically observed in aerosol systems with diffusion limited cluster-cluster aggregation.

Table 2: Burner-stabilized-stagnation-flow flames used for validation of the soot model.

Fuel	Flame	Equivalence ratio	Max. Temperature (K)
Ethylene	C6	2.07	1800
n-Heptane	F1	2.07	1760
n-Heptane	F3	2.07	1940
Toluene	G5	1.73	2000

Before comparing soot predictions with experimental data, temperatures and gas-phase soot precursors were first compared with data to ensure that the gas-phase mechanism predictions and heat transfer were accurately represented by the flame model. Figure 3 shows representative gas-phase species profile comparisons for a toluene flame. As shown in the schematic in Figure 2, H_p refers to the separation distance between the burner surface and the stagnation plate.

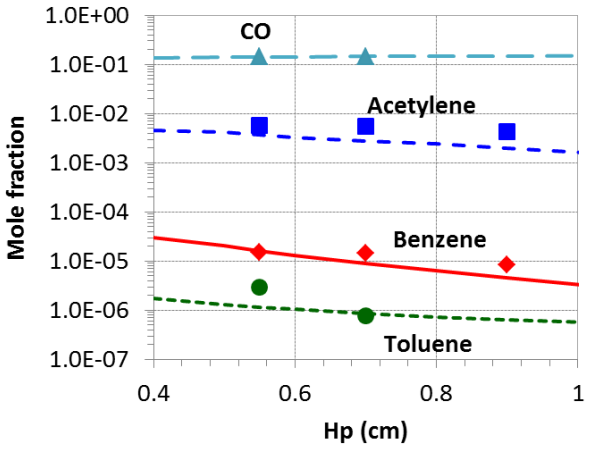

Figure 3: Comparing predicted species profiles for major products, hydrocarbon intermediates and soot precursors with experimental data, for a toluene flame (G5). Symbols represent experimental data from USC and lines represent simulation results.

Figure 4 shows the evolution of soot size distribution for an ethylene fuel 'C6' BSSF flame. The first plot is for a separation distance between the burner surface and the stagnation plane of 0.6 cm, while the second plot is for 2 cm separation distance. The experimental data are from USC [24, 25]. At the smaller separation distance of 0.6 cm, a nucleation tail is formed with large number densities (~10^{11} particles/cm^3) of <20 nm small soot particles. With increasing separation distance and the resultant longer residence time, the particles grow in size to as large as 150 nm. The soot size distribution evolves to a bimodal distribution (it may be noted that the experiments could not measure particles below ~2 nm). The model captures these trends well. The discrepancies at any given separation distance needs to be considered in the context of typical measurement uncertainties. Several factors play roles in the evolving particle size distribution: soot nucleation chemistry continues to create small-sized particles; soot growth

chemistry results in larger particles with the same particle number density; soot oxidation chemistry results in smaller particles and decreased particle number density; soot coagulation and aggregation result in larger particles with reduced particle number densities. These effects are captured well by the model.

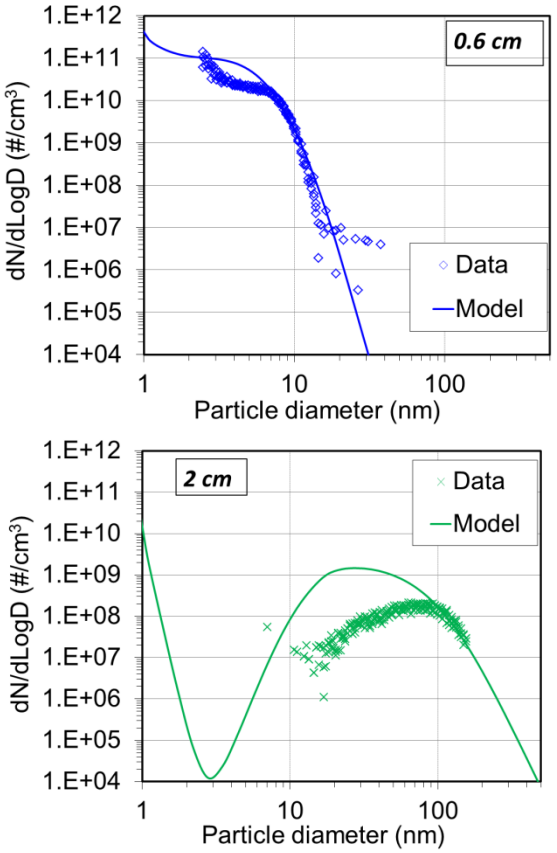

Figure 4: Evolution of soot size distribution with increasing separation distance between burner and stagnation plane, for an ethylene 'C6' BSSF flame.

Figure 5 and Figure 6 show the soot size distributions for two *n*-heptane flames. The main difference between the two flames is the peak flame temperature, as listed in Table 2. The 'F1' flame (peak temperature =1760 K) is cooler than the 'F3' flame (peak temperature =1940 K). The model captures well the soot size distribution for both of these *n*-heptane flames. Figure 5 shows the model being able to capture the bimodal particle distribution that includes the nucleation tail. The data show that the cooler flame produces larger diameter soot particles than the hotter flame, and the model is able to reproduce this effect.

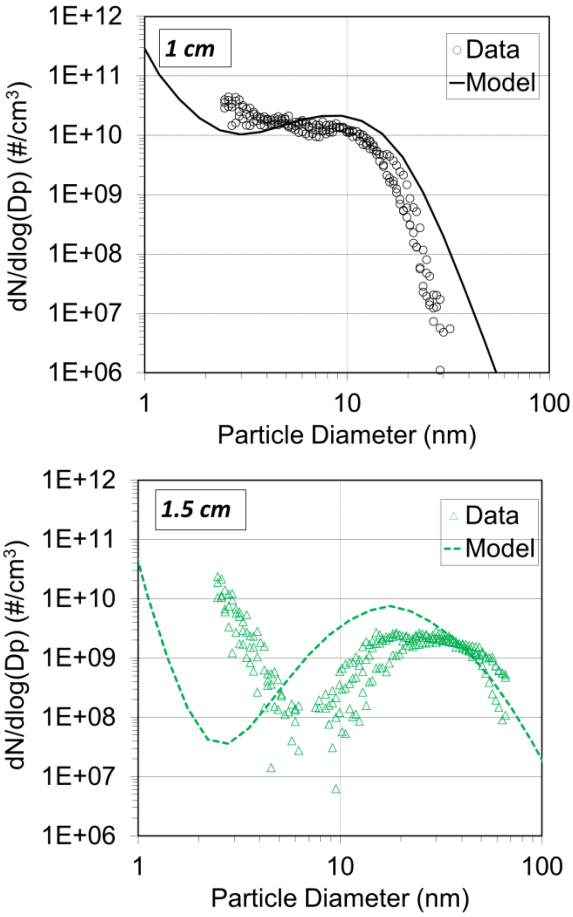

Figure 5: Evolution of soot size distribution with increasing separation distance between burner and stagnation plane, for an *n*-heptane 'F1' BSSF flame.

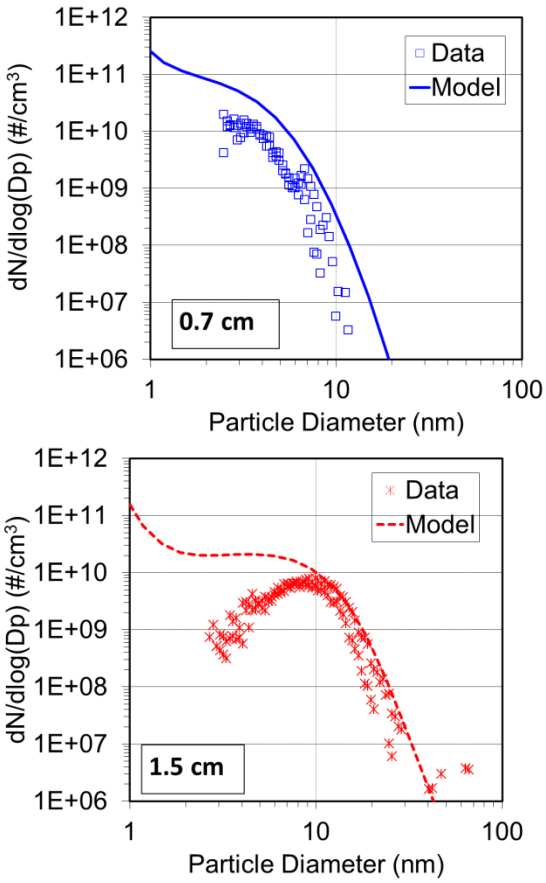

Figure 6: Evolution of soot size distribution with increasing separation distance between burner and stagnation plane, for an *n*-heptane 'F3' BSSF flame.

The BSSF simulations employ a simple aggregation model that assumes a fixed primary particle diameter of 20 nm and a fractal dimension of 1.8. There is some uncertainty regarding these inputs. Figure 7 below shows the impact of modifying these inputs. These results suggest that, for strongly sooting conditions such as those reported here, the aggregation model input uncertainties have a minor impact on the results.

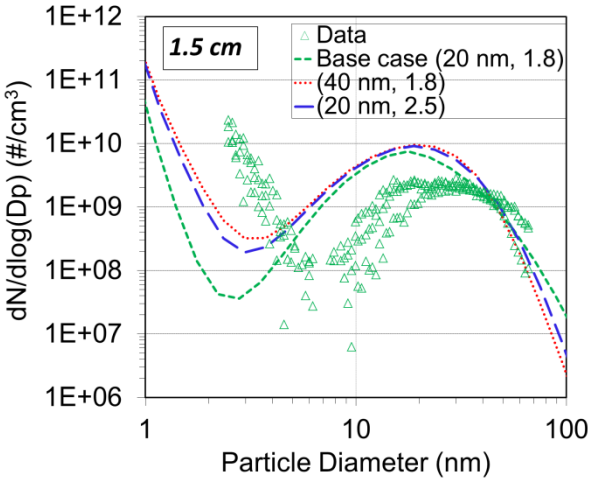

Figure 7: The impact of varying aggregation model parameters on soot size distribution for an *n*-heptane F1 flame. The legend indicates the primary particle diameter and the fractal dimension for the soot aggregation model.

The soot size distribution for a toluene 'G5' flame is shown in Figure 8. The size distributions are shown for separation distances of 0.55 and 0.8 cm. For the toluene BSSF flame simulation alone, the equivalence ratio was changed slightly from the value shown in Table 2, within experimental uncertainty to a value of 1.83.

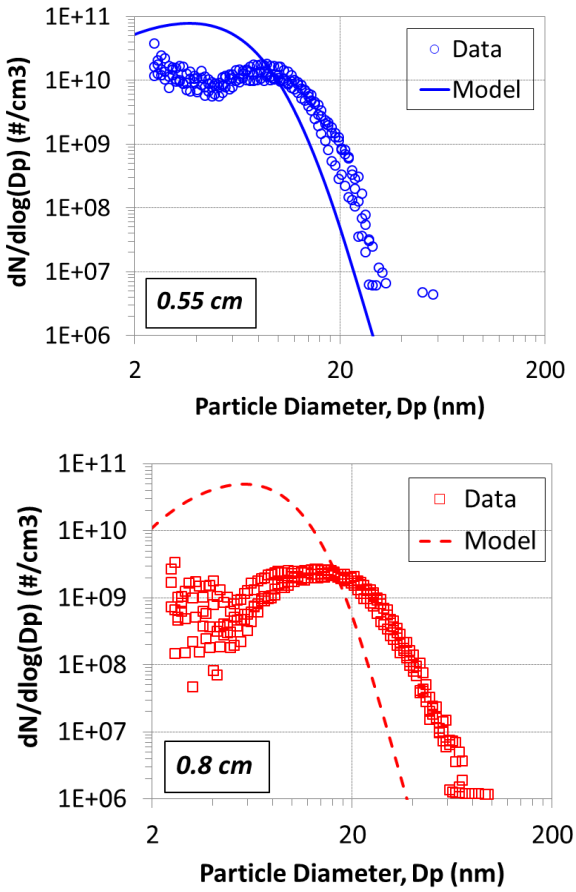

Figure 8: Evolution of soot size distribution with increasing separation distance between burner and stagnation plane, for a toluene 'G5' BSSF flame.

Validation using plug-flow reactor data

In addition to the experimental data from the USC facility, other published data for soot experiments were used to test model predictions. For these simulations, the method of moments was used in CHEMKIN-PRO, since particle size distribution did not have to be modeled. Figure 9 shows soot volume fractions in comparison with the experimental data of Skjøth-Rasmussen et al. [26]. The three figures use varying equivalence ratios (2.66, 3.33, 8) and inlet H_2O amounts (0-0.26 mol %). Over these wide ranges of conditions, the model is able to provide consistent agreement with the data.

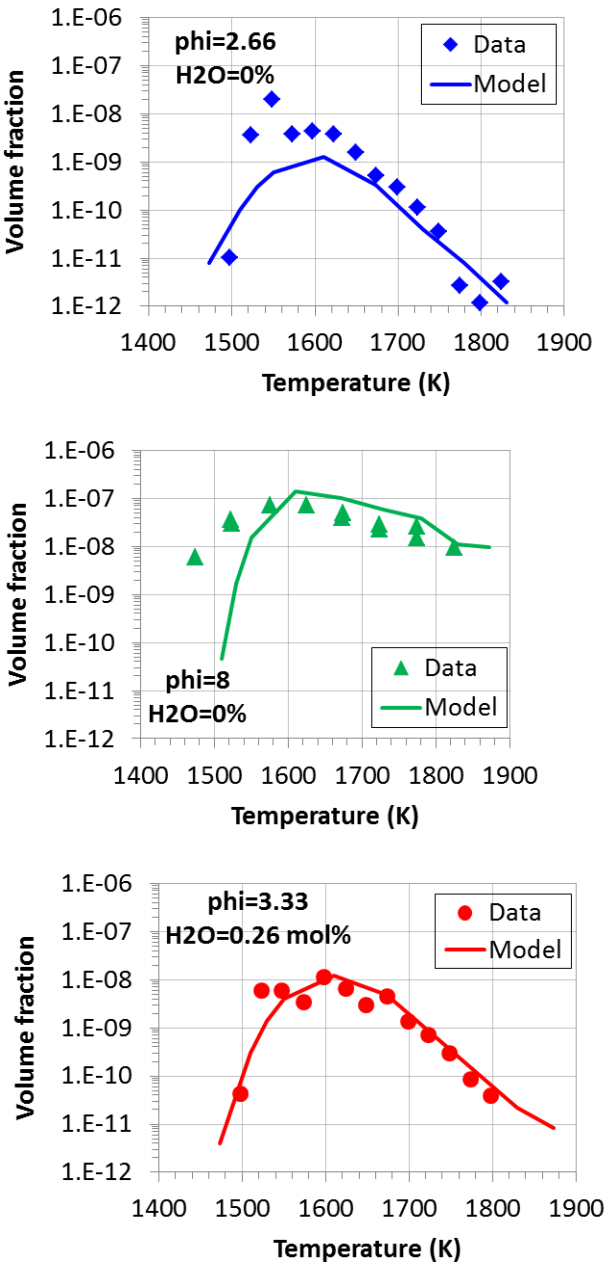

Figure 9: Calculated soot volume fractions in a flow reactor over a range of temperatures, in comparison with experimental data of Skjøth-Rasmussen et al.

Validation using shock-tube reactor data

Figure 10 shows experimental data of soot yield from high-pressure shock tubes of Hong et al. [27] and Kellerer et al. [28]. The pressures of 30–50 bar are a good compliment to the atmospheric-pressure validation data presented earlier. The figure shows a substantial impact of increasing pressure from 30 to 50 bar. The predictions at 30 and 50 bar agree well with the experimental data of Hong et al. and Kellerer et al. The experimental conditions included *n*-heptane as the fuel at an equivalence ratio of 5, with 99% argon dilution. The

simulations were performed for 2 ms of physical time, in accordance with the reaction times used by Hong et al. Kellerer et al. did not specify an end time, but it is estimated to be on the order of ~2 ms. At 30 bar, experimental data scatter can be seen between Hong et al. and Kellerer et al. The data of Hong et al. has a narrower temperature range than the data of Kellerer et al. Within this data scatter, the predictions agree well with the experimental data.

For these experiments, soot yield is defined as the percentage conversion of fuel carbon into soot carbon, as shown in the equation below. The concentrations are in the units of moles/m^3.

$$Yield\ (\%) = \frac{[\mathrm{C}]_{soot}}{[\mathrm{C}]_{total}} \times 100$$

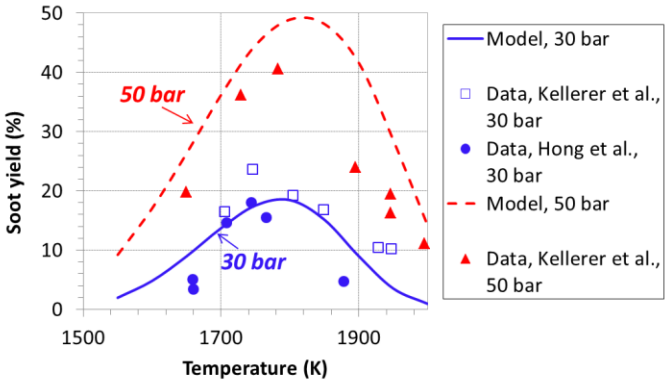

Figure 10: Soot yield predictions at 30 and 50 bar, in comparison with experimental data from Hong et al. and Kellerer et al.

Another test for the soot model at high pressures is for soot induction delay times. The experiments of Mathieu et al. [29] used toluene as the fuel and operated under pyrolysis conditions, with 99.75% argon dilution. For the data shown in Figure 11, while varying the temperature, the pressure was also varied such that a constant 10^{18} carbon atoms/cm^3 fuel feed was maintained for all cases. This translated to pressures of ~10 to 20 atm.

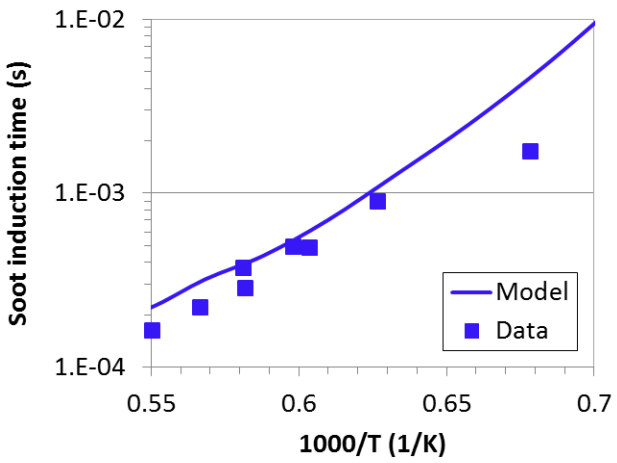

Figure 11: Soot induction delay time predictions compared with the experimental data of Mathieu et al.

Soot oxidation

Experiments were conducted at the USC facility to study soot oxidation by molecular oxygen. Soot oxidation was studied by first generating nascent soot from BSSF flames. The nascent soot particles were then diluted and suspended in a carrier flow of nitrogen and mixed with a high-temperature stream of nitrogen or oxygen/nitrogen mixture and passed through an isothermal flow reactor. Thus, in the flow reactor, only soot oxidation could occur and no soot formation could occur [25, 30]. The amount of oxygen in the flow reactor was varied. These experiments were modeled using the CHEMKIN-PRO plug-flow reactor model [23]. The experiments were designed to maintain the temperature across the flow tube at a nearly constant value throughout the length of the flow reactor, and these measured temperature values were used in the simulations. The sectional model option was used for the particle tracking, with diameters ranging up to 200 nm and a section spacing factor of 1.14. In the results reported here, the aggregation model was used with a fixed primary particle diameter of 20 nm and a fractal dimension of 1.8. The measured soot size distribution at the start of the flow reactor was provided as input to the model, and the evolution of the soot particles was simulated.

Figure 12 shows the impact of oxygen content on the soot particle size distribution for soot particles generated from a rich *n*-heptane flame. The size distribution at both the flow reactor inlet and outlet are shown in the figure. The length of the reactor is 89 cm, which translates to a residence time in the flow reactor of about 0.23 s. The model agrees well with the measurements, with respect to the degree of oxidation and the shift of the particle size distribution that occurs as a result. The average diameter of the soot particles at the inlet was 13 nm. With 4500 ppm oxygen, the predicted average soot particle diameter at the outlet decreased to 10.2 nm. With even more oxygen at 7800 ppm oxygen, the predicted average soot particle diameter at the outlet decreased to 8.2 nm, which compares well to the experimentally measured value of 8 nm. Since the

soot mass/volume fraction is related to diameter[3], these reductions in particle diameters due to oxygen are significant.

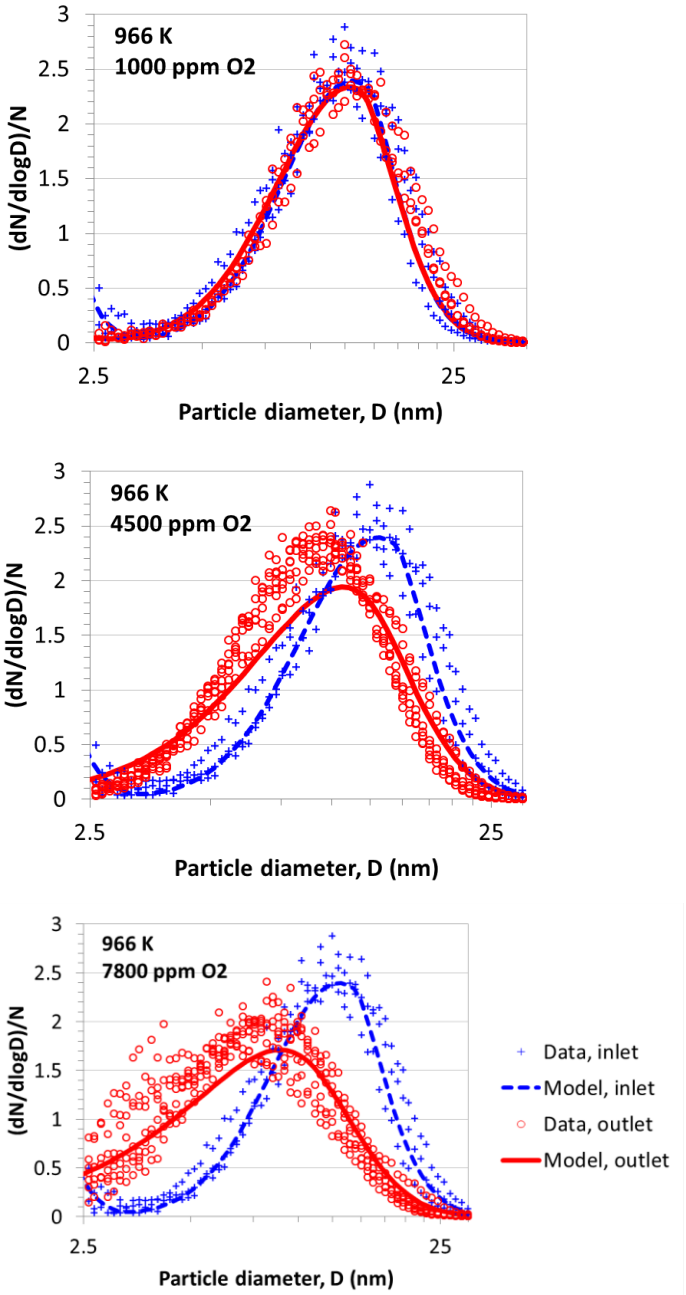

Figure 12: Effect of oxygen concentration on the evolution of soot particle size distribution at 966 K, in comparison with USC experimental data.

Due to experimental constraints, the temperature range in the experiments was restricted to ~950 to 1050 K. Computed soot particle size distributions in Figure 13 show that the model is able to capture the influence of temperature on the oxidation of soot and the resulting changes to the particle size distribution. The plots in Figure 12 and Figure 13 indicate the number of particles decreasing with increasing oxygen content and temperature. The reason for this is that some of the particles are consumed by oxidation. The simulation results agree with the experimental data for this trend in Figure 12; the data shows sizeable scatter for the 1054 K plot in Figure 13.

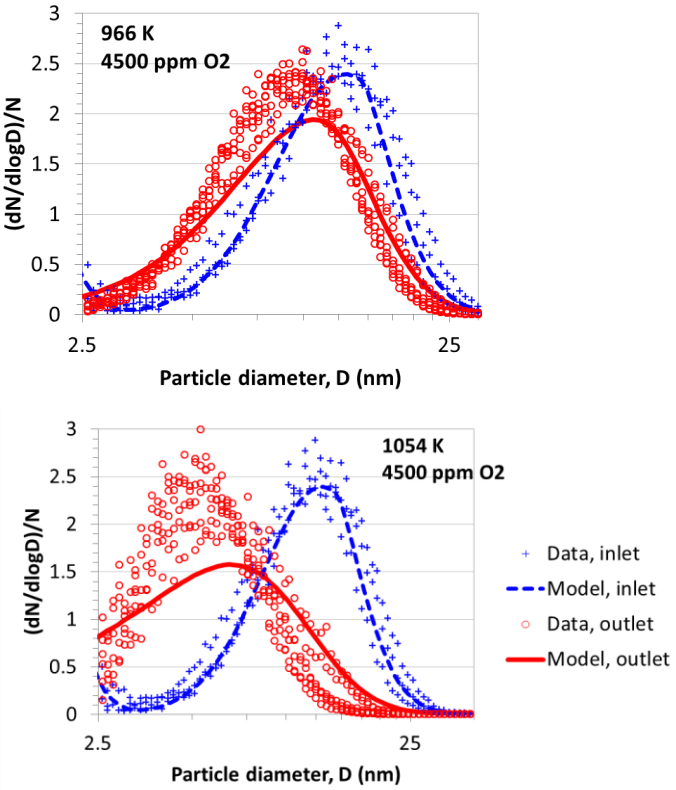

Figure 13: Effect of temperature on the evolution of soot particle size distribution with 4500 ppm oxygen in the inlet, in comparison with USC experimental data.

Another way to look at the validity of the soot oxidation mechanism is to compare the overall consumption of soot mass by oxidation. Figure 14 shows this comparison while varying oxygen concentration in the inlet and the reactor temperature. The model agrees well with the experiment over the range of temperature and oxygen concentration.

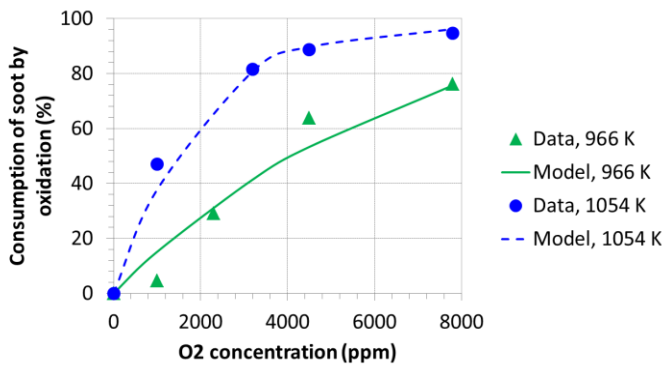

Figure 14: Consumption of soot by oxidation, as a function of oxygen concentration and temperature, in comparison with USC experimental data.

It may be noted that the same soot mechanism was used for all the BSSF, plug-flow reactor and shock-tube reactor simulations presented in this paper.

In this paper, we focused on validation data from fundamental laboratory experiments; this was because these experiments have lesser uncertainties from other factors such as turbulence. From these types of experiments, we had limited data under conditions where both soot formation and oxidation were equally important. However, we focused on both experiments where soot formation dominates and on experiments where soot oxidation dominates. Taken together, we have confidence that the soot mechanism should work well in turbine conditions where both formation and oxidation are relevant.

CONCLUSIONS

A detailed chemistry model has been developed for the soot formation and oxidation chemistry, with a focus on the soot-particle surface kinetics. Through collaboration with the University of Southern California, the model has been developed and validated against a unique set of soot data measured in flames for several single-component fuels. In addition to soot growth, soot oxidation through molecular oxygen was also improved and validated based on the USC data. The chemistry in the soot surface model includes particle nucleation, growth through the HACA (hydrogen-abstraction/carbon-addition) and PAH-condensation (polycyclic aromatic hydrocarbons) pathways, as well as soot-oxidation pathways. In addition to soot chemistry, the physics of particle coagulation and aggregation were included in the model. The results demonstrate the ability of well-validated chemistry to predict both dramatic and subtle effects related to soot modeling.

The validation shows the model performing well under flame, flow-reactor and high-pressure shock-tube conditions. A range of conditions were considered, including effects of varying fuels (ethylene, *n*-heptane, toluene), temperatures (~1000-2000 K), pressures (1-50 atm), equivalence ratios (1.7-8) and residence times. Observed effects of these factors on the soot particle size distribution shape and soot quantity were reproduced by the model. The good validation results give confidence in using the soot model for conditions of interest in turbines and other engines. The accurate soot model can be used directly in CFD when a particle-tracking capability is included in the CFD simulation [18], or as part of an equivalent reactor network approach [20].

ACKNOWLEDGMENTS

This work has been partially supported by the Model Fuels Consortium II [6]. We also thank Prof. Hai Wang and Joaquin Camacho for providing experimental data and for helpful discussions.

REFERENCES

1. Samuelsen, G.S. *http://www.ucicl.uci.edu/2/RESEARCHPROJECTS/EMISSIONS/RichBurnQuickMixLeanBurn/EMISSIONS-RichBurnQuickMixLeanBurn.pdf*.
2. Dagaut, P. and M. Cathonnet, *The Ignition, Oxidation, and Combustion of Kerosene: A Review of Experimental and Kinetic Modeling.* Progress in Energy and Combustion Science, 2006. **32**.
3. Colket, M., et al., *Development of an Experimental Database and Kinetic Models for Surrogate Jet Fuels*, in *45th AIAA Aerospace Sciences Meeting*2007, AIAA: Reno, NV.
4. Pitz, W.J., N.P. Cernansky, F.L. Dryer, F. Egolfopoulos, J.T. Farrell, D.G. Friend, and H. Pitsch, *Development of an Experimental Database and Chemical Kinetic Models for Surrogate Gasoline Fuels.* SAE Technical Papers, 2007. **2007-01-0175**.
5. Farrell, J.T., N.P. Cernansky, F.L. Dryer, C.A. Hergart, C.K. Law, R.M. McDavid, C.J. Mueller, A.K. Patel, and H. Pitsch, *Development of an Experimental Database and Kinetic Models for Surrogate Diesel Fuels.* SAE Technical Papers, 2007. **2007-01-0201**.
6. http://www.modelfuelsconsortium.com *Reaction Design Launches Automotive Fuels Consortium*. PR Newswire, 2006.
7. Puduppakkam, K.V., C.V. Naik, C. Wang, and E. Meeks, *Validation Studies of a Detailed Kinetics Mechanism for Diesel and Gasoline Surrogate Fuels.* SAE Technical Paper 2010-01-0545, 2010.
8. Naik, C.V., K. Puduppakkam, and E. Meeks, *Modeling the Detailed Chemical Kinetics of NOx Sensitization for the Oxidation of a Model fuel for Gasoline.* SAE International Journal of Fuels and Lubricants 2010. **3**(1): p. 556-566.
9. Naik, C.V., K.V. Puduppakkam, C. Wang, J. Kottalam, L. Liang, D. Hodgson, and E. Meeks, *Applying Detailed Kinetics to Realistic Engine Simulation: The Surrogate Blend Optimizer and Mechanism Reduction Strategies.* SAE International Journal of Engines, 2010. **3**(1): p. 241-259.

10. Naik, C.V., K.V. Puduppakkam, and E. Meeks, *An improved core reaction mechanism for C0-C4 unsaturated fuels and C0-C4 fuel blends*, in *Proceedings of ASME Turbo Expo 2012, GT2012*2012: Copenhagen, Denmark.
11. Naik, C.V., K.V. Puduppakkam, and E. Meeks, *An improved core reaction mechanism for saturated C0-C4 fuels.* Journal of Engineering for Gas Turbines and Power, 2011. **134**(2).
12. *Reaction Workbench 15131*, 2013, Reaction Design, San Diego.
13. Skjøth-Rasmussen, M.S., P. Glarborg, M. Østberg, J.T. Johannessen, H. Livbjerg, A.D. Jensen, and T.S. Christensen, *Formation of polycyclic aromatic hydrocarbons and soot in fuel-rich oxidation of methane in a laminar flow reactor.* Combustion and Flame, 2004. **136**: p. 91–128.
14. Raj, A., M. Celnik, R. Shirley, M. Sander, R. Patterson, R. West, and M. Kraft, *A statistical approach to develop a detailed soot growth model using PAH characteristics.* Combustion and Flame 2009. **156**: p. 896–913.
15. Wang, H. and M. Frenklach, *A Detailed Kinetic Modeling Study of Aromatics Formation in Laminar Premixed Acetylene and Ethylene Flames.* Comb. Flame, 1997. **110**: p. 173-221.
16. Appel, J., H. Bockhorn, and M. Frenklach, *Kinetic Modeling of Soot Formation with Detailed Chemistry and Physics: Laminar Premixed Flames of C_2 Hydrocarbons.* Combustion and Flame, 2000. **121**: p. 122-136.
17. Nagle, J. and R.F. Strickland-Constable. *Oxidation of Carbon Between 1000-2000 C*. in *Fifth Carbon Conference*. 1962.
18. *FORTÉ 40132*, 2013, Reaction Design, San Diego.
19. Drennan, S.A., C.-P. Chou, A.F. Shelburn, D.W. Hodgson, C. Wang, C.V. Naik, E. Meeks, and H. Karim. *Flow Field Derived Equivalent Reactor Networks for Accurate Chemistry Simulation in Gas Turbine Combustors*. in *ASME Turbo Expo 2009: Power for Land, Sea, and Air, GT2009-59861*. 2009. Orlando, Florida, USA.
20. *ENERGICO 30131*, 2013, Reaction Design, San Diego.
21. Abid, A.D., J. Camacho, D.A. Sheen, and H. Wang, *Evolution of Soot Particle Size Distribution Function in Burner-Stabilized Stagnation n-Dodecane−Oxygen−Argon Flames.* Energy Fuels, 2009. **23**(9): p. 4286–4294.
22. Abid, A.D., J. Camacho, D.A. Sheen, and H. Wang, *Quantitative measurement of soot particle size distribution in premixed flames-- The burner-stabilized stagnation flame approach.* Comb. Flame, 2009. **156**(10): p. 1862–1870.
23. *CHEMKIN-PRO 15131*, 2013, Reaction Design, San Diego.
24. Wang, H. and J. Camacho, *Personal Communication*, 2012.
25. Camacho, J. and H. Wang. *Kinetics of Nascent Soot Oxidation in a Flow Reactor*. in *8th U. S. National Combustion Meeting*. 2013.
26. Skjøth-Rasmussen, M.S., P. Glarborg, M. Østberg, J.T. Johannessen, H. Livbjerg, A.D. Jensen, and T.S. Christensen, *Formation of polycyclic aromatic hydrocarbons and soot in fuel-rich oxidation of methane in a laminar flow reactor.* Combustion and Flame, 2004. **136**: p. 91-128.
27. Hong, Z., D.F. Davidson, S.S. Vasu, and R.K. Hanson, *The effect of oxygenates on soot formation in rich heptane mixtures: A shock tube study.* Fuel, 2009. **88**: p. 1901–1906.
28. Kellerer, H., A. Muller, H.-J. Bauer, and S. Wittig, *Soot Formation in a Shock Tube under Elevated Pressure Conditions.* Combustion Science and Technology, 1996. **113-114**: p. 67-80.
29. Mathieu, O., G. Frache, N. Djebaili-Chaumeix, C.-E. Paillard, G. Krier, J.-F. Muller, F. Douce, and P. Manuelli, *Characterization of adsorbed species on soot formed behind reflected shock waves.* Proceedings of the Combustion Institute, 2007. **31**: p. 511–519.
30. Camacho, J. and H. Wang, In Preparation for Proceedings of the Combustion Symposium, 2014.